EXEP: Mountaintop Starshade Concept Study

Stefan Martin, Stuart Shaklan, B. Mennesson, R. Capps
Jet Propulsion Laboratory
California Institute of Technology
4800 Oak Grove Dr.
Pasadena, CA 91109
stefan.r.martin@jpl.nasa.gov

***Abstract*—Starshades are external occulters which would be used in conjunction with a space telescope. The starshade has a particular apodizing profile that effects strong suppression of starlight within the starshade's shadow. Since starshades that would be used in space are large, typically 30 m diameter, performance is difficult to test on the ground at realistic scales. This paper examines the practical limits for testing starshades at smaller scales in the atmosphere and goes on to describe concepts for testing starshades using ground based telescopes and using starshades for astronomical observations**

TABLE OF CONTENTS

1. INTRODUCTION

Starshades are being studied as external occulters flown ahead of a space telescope. In appearance somewhat like a sunflower with a central disc and radial petals, the petals are shaped to admit a minimal amount of the starlight into a shadow region behind the shade. Starshades that are designed to enable the study of exoplanets in the habitable zone around nearby stars are necessarily large, typically 30 m or more in diameter, and positioned a long way from the telescope, typically 30 Mm or more. These scales are dictated by the desire to achieve a small inner working angle (IWA) which, in turn, dictates a small diffraction angle of the starlight around the shade so that the shade becomes large and the telescope retreats. Because of these large scales, demonstrating starshades at realistic sizes on the ground is impractical, so subscale tests become a necessity if diffraction models of starshade performance are to be validated.

Figure 1 summarizes the current state of the art in ground tests ranging from small scale laboratory tests over a few meters to larger scales of a kilometer or so in desert tests. Successful modeling of actual performance in the lab (Ref. 1) has provided some confidence in the performance predictions over the small scale, and current work aimed at resolving disagreements (particularly with respect to starshade shape defects) between the handful of models available, is bearing fruit. To reach longer distances and to use larger diameter shades requires operation outdoors or in long, wide tunnels. The NGAS desert tests (Ref. 2) have demonstrated the capability to get useful information in the presence of atmospheric disturbances and windblown dust, but Fresnel numbers have been large compared to space, so two important goals of new experiments are to increase the starshade size and reduce the Fresnel number and hence operate over a larger range.

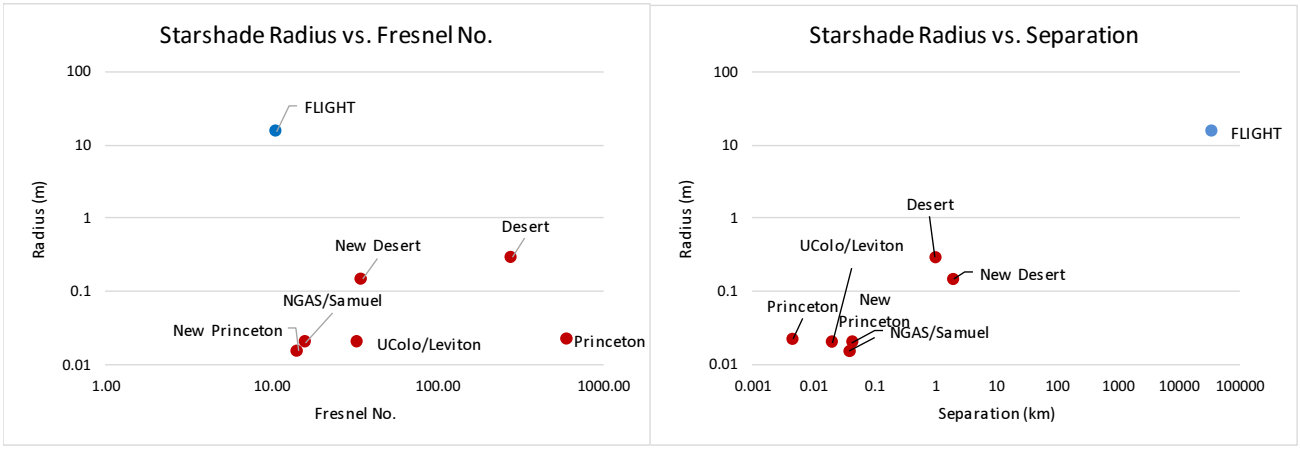

Figure 1: Current state of the art in ground tests. Left: Starshade radii do not exceed 0.3 m while Fresnel numbers are generally much larger than flight. Right: Starshade-telescope separations are well below the space case. The data are derived from references detailed in Appendix A, with some assumptions made as necessary.

978-1-5090-1613-6/17/$31.00 ©2017 IEEE

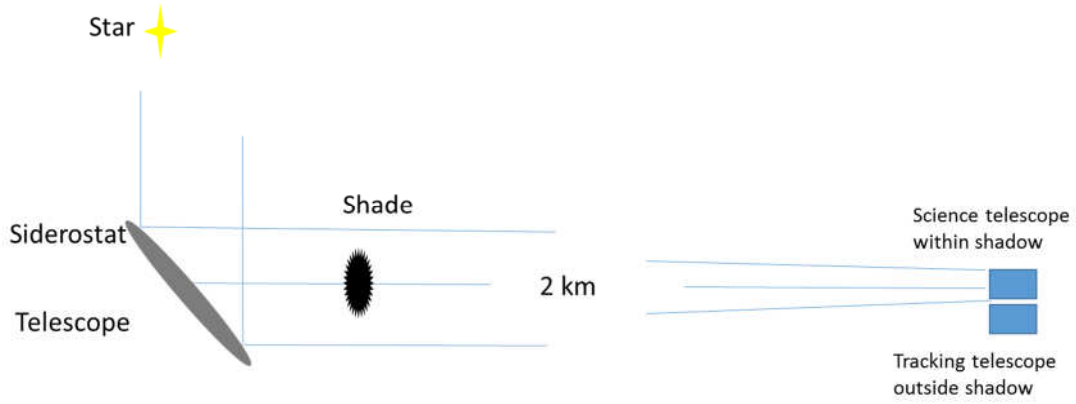

Figure 2: Setup for an outdoor starshade test using a large siderostat mirror.

Figure 1 illustrates the difference between the operating regime in flight and in tests so far, by comparing starshade radius against Fresnel number and against separation. Some tests have Fresnel numbers approaching flight, but with very small starshades (Fig. 1 left), while tests using larger starshades have fallen short on range.

To test optical models on the ground at an intermediate scale between space (30,000 km) and desert (1 km) is a challenge. As an extreme example of line of sight on the ground: from Mount Diablo in northern California, Lassen Peak can sometimes be observed at a range of almost 300 km, but this requires unusually clear atmospheric conditions.

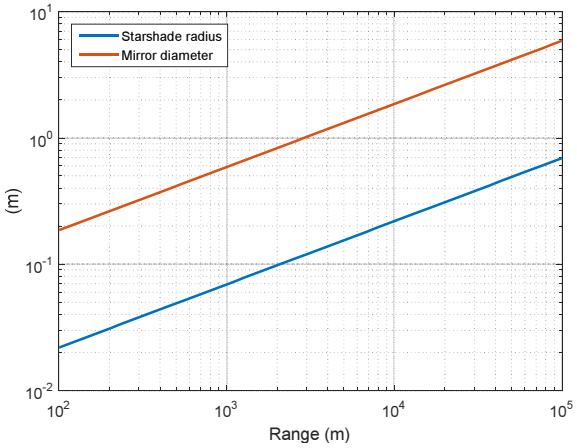

Figure 3: Siderostat mirror diameter and starshade radius for a Fresnel number of 8, OWA/IWA = 3 with siderostat tilt of 45 degrees.

Ideally, the light source placed behind the starshade would be very distant. In the desert tests, the light source is equidistant from the shade as the telescope, but this creates a significantly diverging beam at the shade, rather than the plane wavefront from a star. This can be accounted for by adjusting the Fresnel number, but it is yet one more difference to be modeled; a star would be a more appropriate source. To direct starlight onto the shade, a siderostat mirror much larger than the starshade would be needed to follow the star's sidereal motion. Figure 2 shows such a setup for a 2 km test. The shade is mounted close to the siderostat mirror and the telescope is positioned 2 km away. A star-tracking telescope is placed next to the science telescope, far enough off axis to see the unobscured star. To account for slow beam drift from large scale eddies, the star tracker provides input to a feedback loop that controls the siderostat pointing.

To fully utilize a 300 km range at a flight-like Fresnel number (א) of 8, a 1.2 m radius starshade would be required: $r=\sqrt{(א\lambda Z)}$, with Z the range and λ the wavelength, here 600 nm. The IWA = $\sqrt{(א\lambda/Z)}$ would be 0.8 arc sec in the absence of atmospheric effects discussed below. Buck (Ref. 3) made measurements of laser beam propagation over a 145 km range in Colorado. Based on this, a line of sight of 50 km to or from a far off high point, making for a starshade radius of 0.45 m or so, would seem practical. For illustration, Figure 3 shows how starshade size will grow with range for a space-like Fresnel number and how large the siderostat mirror would be with a 45 degree siderostat tilt and a modest outer working angle (OWA). Already at 10 km range the siderostat would be ~ 6 m diameter. This illustrates a restriction compared to the space case: whereas in space the outer working angle is unrestricted, on the ground the siderostat edge places a limit.

To achieve good image plane contrast, diffraction from the edge of the siderostat mirror needs to be managed, so this is a significant difference from the space case. Figure 4 shows a suspended starshade (lower left) designed for a long ground based testbed (10s of meters). This shade consists of an inner starshade connected to an outer starshade whose function is to mechanically suspend the inner shade but also to produce an apodization to the edge of the aperture, thus attenuating the edge diffraction. The rightmost column in the figure compares the ring of light diffracted from the siderostat edge with and without the apodizing suspension. The difference in the focal plane contrast is about 2000.

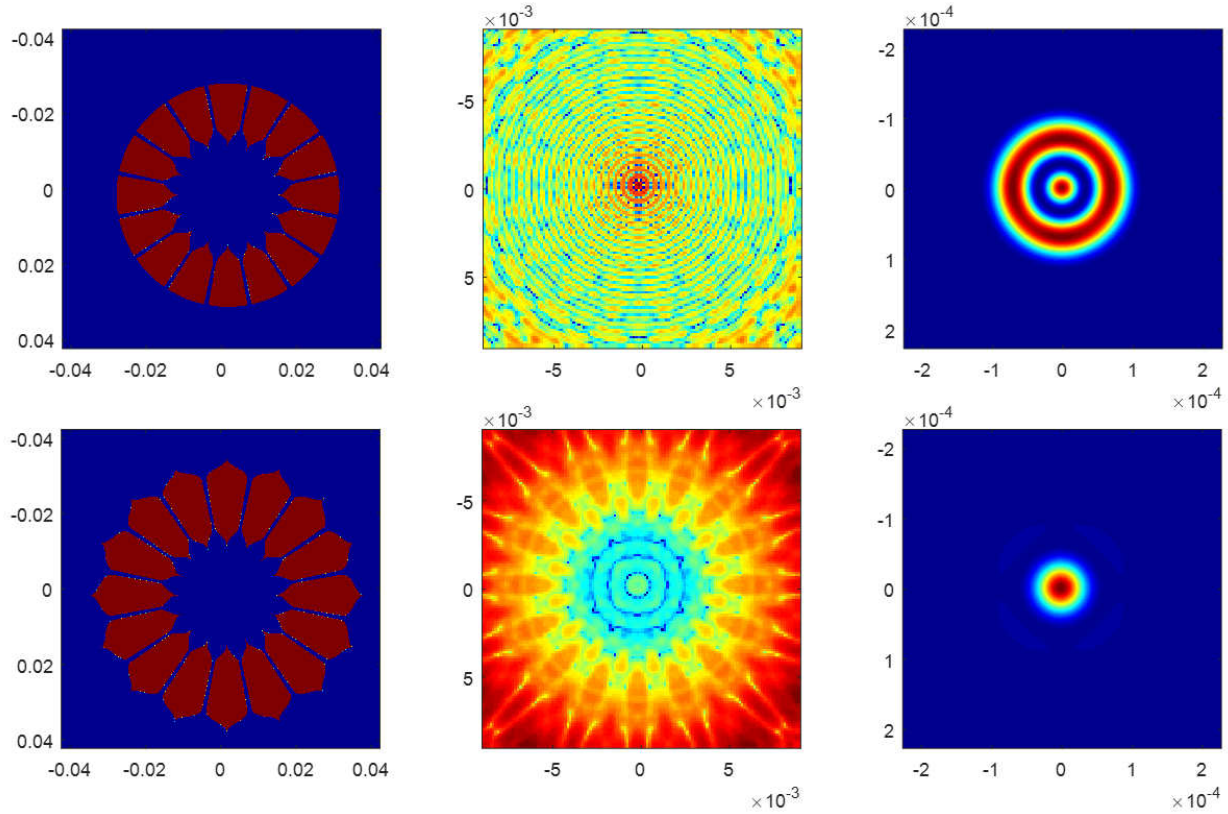

Figure 4: Upper, a small suspended shade with a circular outer edge. Lower, the same shade with an apodizing outer edge designed for a 70 m long tunnel. Left to right: Mask shape (red areas transmit light), pupil plane and image plane intensity distributions. Axes are scaled in meters and intensity scales are arbitrary. The center column shows the shadows of the shades at the telescope entrance pupil plane. The topmost image shows rings of light diffracted into the center by the circular mask edge, in stark contrast with the pronounced shadow shown lower center. The entrance pupil for the final image is only 1.5 mm diameter and as a result the edge of the shade is poorly resolved. It can be seen faintly in lower right surrounding the central peak, and much brighter upper right. The peak intensities (relative to the intensity of the unapodized star) in the image planes are $1x10^{-3}$ upper right and ~$5x10^{-8}$ lower right, showing the benefit of the apodized outer edge in improving the image plane contrast.

2. ATMOSPHERIC EFFECTS ON PROPAGATION

Empirical data

Buck gives an empirical formula based on experimental data for propagation of a laser beam under good conditions, 2 km above sea level and 60 m above the surrounding terrain. The measured diameter of the laser beam at 633 nm wavelength was fitted to $D=\alpha Z^{\beta}$ with Z the range, and α and β found to be 4.5×10-6 and 1.2 respectively with units of m. Integration time was 30 s, while over longer periods slow drifting dominated (as much as 4 m at 10 km range). This empirical

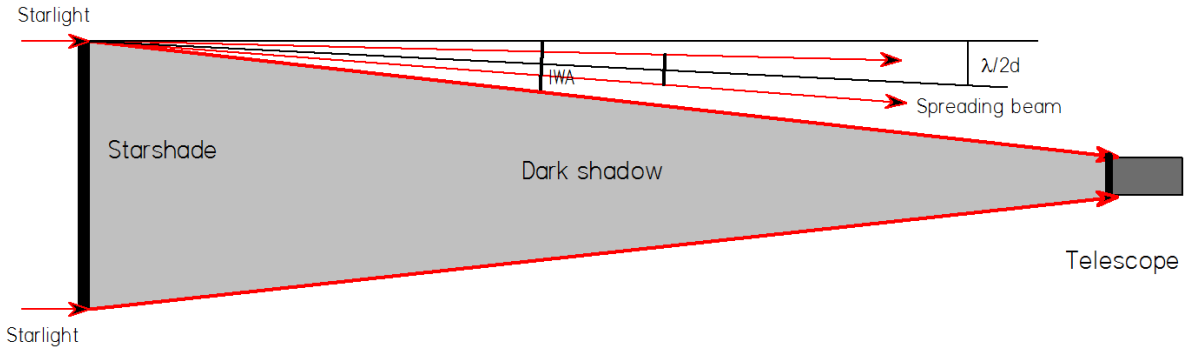

Figure 5: The angular spread of the beam due to seeing.

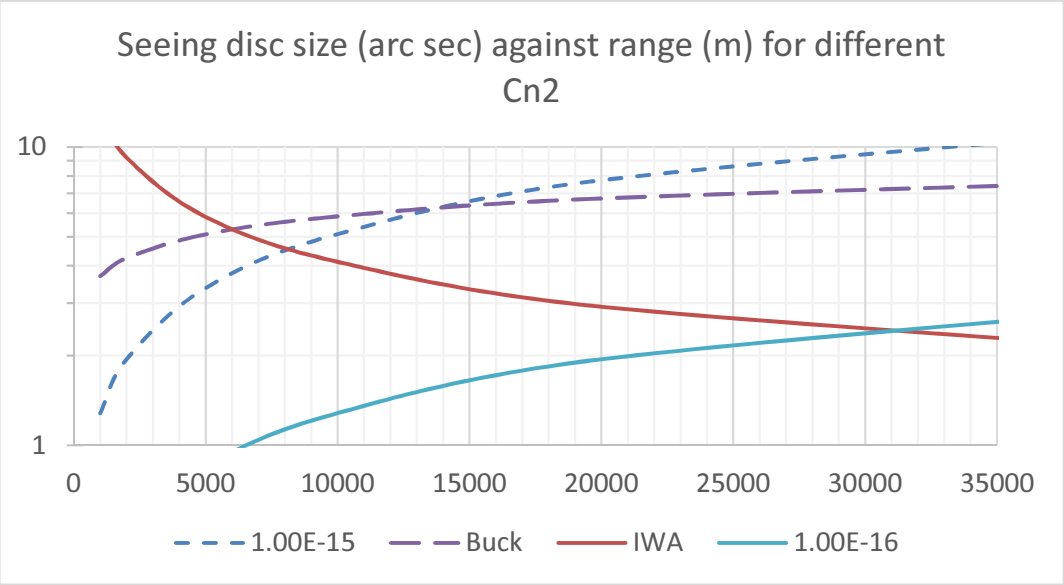

Figure 6: Modeled seeing disc diameter against range across the ground. The dashed blue line approximates an experiment at Mt Wilson under excellent seeing, using r0 ~200 mm, which is possible ~20% of the time. The red line is the minimum IWA against range at 500 nm wavelength. From these two curves we conclude that only starshades utilizing something less than a ~8000 m range are feasible for deep contrast on the ground. Furthermore, the dashed purple line shows Buck's empirical model which indicates that ranges greater than ~6000 m are not feasible.The light blue line shows a 10x better C_n^2 than for the Mt Wilson model line.

formula fitted the data well over paths from 550 m to 145 km. The transmitting aperture had a 10 cm diameter and the laser beam grew in size at a rate much faster than the initial aperture-limited divergence. Since the beam expansion is driven by the turbulence, this is a reasonable proxy for propagation of the beam and shadow from a starshade. (Note also that Buck found at times both α and β could be considerably larger.) The angular radius of the beam is given by $\rho=\alpha Z^{(\beta-1)}/2$.

In the absence of atmospheric turbulence, the light fills in behind the starshade at an angle $\lambda/2d = \lambda/4r$. If the radial spread of the beam $\rho << IWA-\lambda/2d$ where d is the starshade diameter, none of the starlight diffracts into the shadow region and there will be a dark hole behind the starshade as seen in figure 5. With the Fresnel number $\aleph = r^2/\lambda Z$, and the IWA = r/Z, the IWA is also equal to $\aleph\lambda/r$. In other words, to be within the starshade shadow, the IWA is necessarily much greater than the diffraction angle. Therefore ρ and IWA dominate and to avoid scattering light into the shadow, the setup should be designed so that ρ will normally be << IWA. Of course, the intermittent nature of turbulence may allow for occasional dark holes to be observed even if the reverse is the case and the angular radial size of the beam generally exceeds the IWA.

In Table 1, different size starshades are compared for use at Fresnel number of 8 using Buck's formula. In this table, the larger starshades seem infeasible unless a "lucky imaging" strategy is adopted. In fact, none of these starshade setups reaches the criterion ρ << IWA, with the arguable exception of D. The 0.1 m radius starshade over 2 km roughly approximates the New Desert testing scenario (figure 1 and Table 1, row D), so ρ < 5*IWA, would be an empirical estimate.

Table 1: Selected starshade geometries for a wavelength of 600 nm and Fresnel number of 8.

	Siderostat Diameter (m)	Range (m)	Starshade Radius (m)	IWA	Beam Radial Expansion (Buck)	IWA/ρ
A	4.2 m	50,000	0.49	2.0"	4.0"	0.5
B	3.0 m	26,050	0.35	2.8"	3.5"	0.8
C	1.9 m	10,000	0.22	4.5"	2.9"	1.6
D	0.83 m	2,000	0.10	10.1"	2.1"	4.8
E	McMath 2.1 m	12,800	0.25	4.0"	3.1"	1.3
F	McMath 1.8 m	9,400	0.21	4.6"	2.9"	1.6
G	ISI 2.1 m	12,800	0.25	4.0"	3.1"	1.3

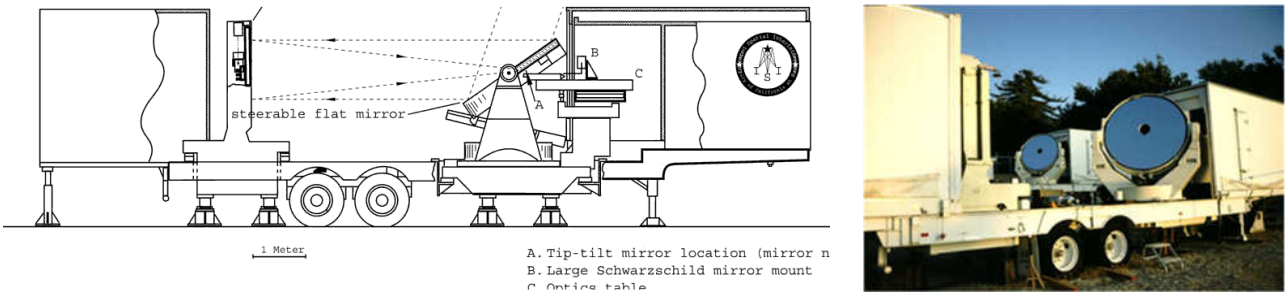

Figure 7: Berkeley Infrared Spatial Interferometer from Ref. 6

Modeling optical propagation

Now we move to an approach based on an atmospheric propagation model. The Fried parameter (r0) is the diameter of a circular area over which the rms wavefront aberration due to the atmosphere is equal to 1 radian, so that the wavefront error is "small" in imaging terms. It is typically quoted at 500 nm and related to the atmospheric turbulence strength C^2_n as follows:

$$r_0 = \left[0.423k^2 \int C_n^2(z)w(z)dz\right]^{-3/5}$$

with *z* the distance along the optical path and *w*(*z*) a weighting function equal to unity for a plane wave. The atmospheric turbulence strength is given by:

$$C_n^2 = \overline{[n(x) - n(x+r)]^2}\, r^{-2/3}$$

with the term in *n*() being the refractive indexes at locations r apart. The refractive index difference arises from temperature gradients in the turbulent atmosphere. The Fried parameter is related to the size of the seeing disc thus: λ/r0, setting a limit on the resolution of a ground-based telescope.

A model of the atmospheric turbulence strength at La Palma (Ref. 4) shows that near ground level the value is typically 10^{-15}, rapidly decreasing with altitude. Figure 6 shows the seeing disc diameter on the detector for C^2_n of 10^{-15} and 10^{-16}. Chosen values of 10^{-15} and z=200 m approximate Mt Wilson (known as the best observatory site in the continental US) under exceptional conditions with a Fried parameter of 0.2 m (Ref. 5). At a range of 2000 m, the seeing disc size (dashed blue line) is already 1.9 arc sec. From the equation for r0 above, the relationship between the seeing disc radius and the range is found to be $\rho=\alpha Z^{\beta}$ with α = 0.01 and β = 0.6, a stronger relationship than found in Buck's experiments. Nonetheless, there is reasonable agreement between the models over ranges from 5 km to 30 km or so. Thus, from figure 6, comparing the red curve with either Buck's curve or the model with $C^2_n = 10^{-15}$, we conclude that something less than between a 6000 m to 8000 m range would be the maximum practicable for a ground based starshade under good atmospheric conditions, corresponding to a starshade diameter of ~0.31 m at ℵ = 8. This range exceeds ground tests to date, but not by much.

3. GROUND IMPLEMENTATIONS

If the horizontal distance on the ground can be reduced, better performance should be achieved, so horizontal starshade and detector layouts are not preferred. Arrangements potentially limited only by the disturbance above the telescope (which typically decreases rapidly with height) can be achieved using conventional ground-based telescopes.

A Virtual Telescope

A positive lens placed immediately after the starshade will cause the light from around the shade to converge almost at the focal distance along the axial direction. A detector placed within the shadow behind the lens and within the focal length, will create a virtual image also behind the lens. From the simple lens formula:

$$v = \frac{fu}{u - f}$$

With for example, f = 70 m and u = 69.9 m, then v = -48930 m, so that, as seen by an observer looking through the lens at the detector, it appears to be a large distance away and greatly magnified. Thus, this arrangement can be used to create a longer apparent path between the starshade and telescope (detector) than is physically the case. The effect of introducing the lens is to create a short system that mimics a much longer path to the telescope, thereby increasing Z. If this shorter path is protected from the strong ground level atmospheric turbulence, the performance of the system can be expected to be much better than that possible using the basic arrangement shown in Figure 2.

Berkeley Infrared Spatial Interferometer Array

The Infrared Spatial Interferometer (ISI) consists of three 1.65m aperture movable Pfund telescopes, located at Mt Wilson Observatory, CA. Figure 7 shows the telescope layout and a photograph of two of the three units that were built. Light from the sky is directed by the siderostat mirror to a paraboloidal primary which focuses the light through a central hole in the siderostat mirror. The light is detected in the cabin at right in the images. The siderostat mirror (~2.1 m diameter) on a single unit of the interferometer could be used to direct light from the sky to an external starshade and telescope. The layout for this detection is shown in Figure 8.

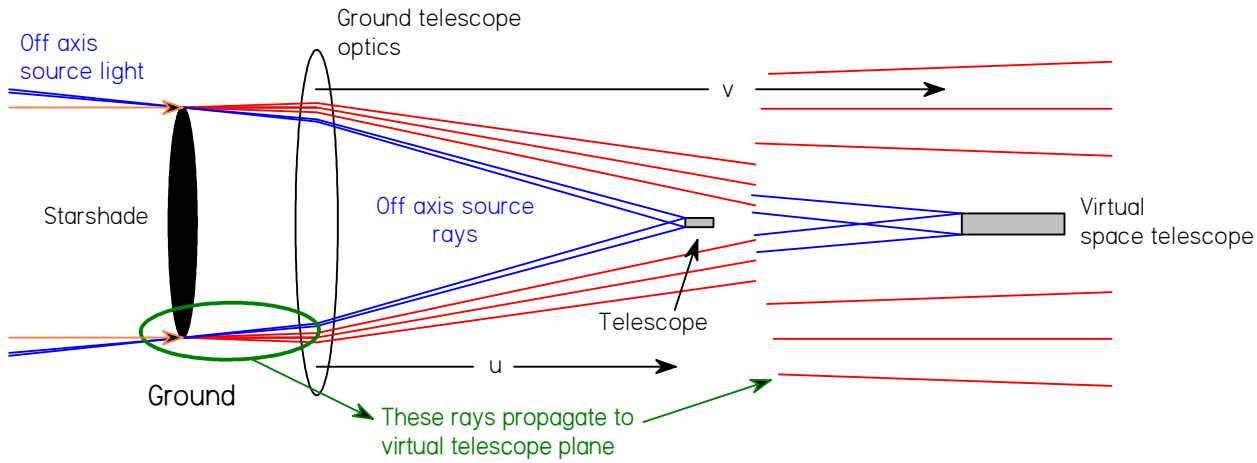

Figure 8: Implementing a starshade using a small telescope inside the focal length of a ground telescope, creating an equivalent larger space telescope at a great distance from the starshade.

The optics mimic the setup for a starshade and detector with a much larger separation, depending on the position of the detector.

With a suspended starshade placed over the parabolic mirror and the detector within the focal length (figure 8 shows the arrangement), the seeing is driven by the vertical path through the atmosphere rather than along a horizontal path, so about 0.5" for excellent conditions at Mt. Wilson and <1.0" typically. With this setup (line G of Table 1), the IWA is 4", so the shadow is 12% to 25% filled by the seeing.

Palomar 200" Hale telescope

At Palomar, the adaptive optics (AO) system can be used to improve the apparent seeing. Under excellent conditions the AO system can return high Strehl (85% or better) images in the near infrared. When using the AO system, starshade detection will be in the infrared (AO uses the visible light) which improves the apparent seeing angle since r0 is proportional to $\lambda^{-1.2}$, but makes the starshade IWA larger $\sim\lambda^{1/2}$. Using 1.8 um radiation and a 1.67 m diameter starshade, the IWA is 3.6". Values of the seeing disc size for PALAO under good conditions range between 0.06" and 0.14" (Ref. 8), suggesting that the shadow will be only slightly filled by the seeing. The AO system corrects mostly the larger scale wavefront errors while high frequency errors contribute a halo around the well corrected ray paths. The magnitude of this halo will set a limit on the ultimate performance. However, the indications are that use of the AO system will permit a high performance starshade experiment. It is also possible to place the starshade within the telescope optical system as shown in Figure 9. The internal shade forms an enlarged virtual shade image ahead of the virtual telescope image.

Assuming, at the larger end, an aperture of 8 m (corresponding approximately to one of the Gemini telescopes), then the starshade could be as large as 2.7 m diameter, much less than the space case, but still superior to experiments so far. With a 2.7 m starshade and a Fresnel number of 8, the virtual telescope is located more than 100 km behind the shade (compare to Exo-S 40 Mm, Ref. 12). The IWA reaches 1.5 arc sec at a wavelength of 1.2 micron. Table 2 shows a few combinations of aperture and wavelength utilizing three existing telescopes. Since PALAO operates on the visible wavelengths, some wavefront correction is obtained at the shorter end of the infrared, so that under good conditions, 1.2 um may be usable.

Table 2: Telescope and starshade combinations. ISI data assumes use of Pfund telescope.

	Aperture (m)	Shade D (m)	Z (m)	IWA (as)	OWA (as)	Wavelength (m)
Hale 200"	5	1.8	56,300	3.3	9.2	$1.8\ 10^{-6}$
Hale 200"	5	1.8	84,400	2.2	6.1	$1.2\ 10^{-6}$
Gemini	8	2.7	123,000	2.2	6.7	$1.8\ 10^{-6}$
Gemini	8	2.7	185,000	1.5	4.5	$1.2\ 10^{-6}$
ISI	1.7	0.57	16,700	3.5	10.5	$0.6\ 10^{-6}$

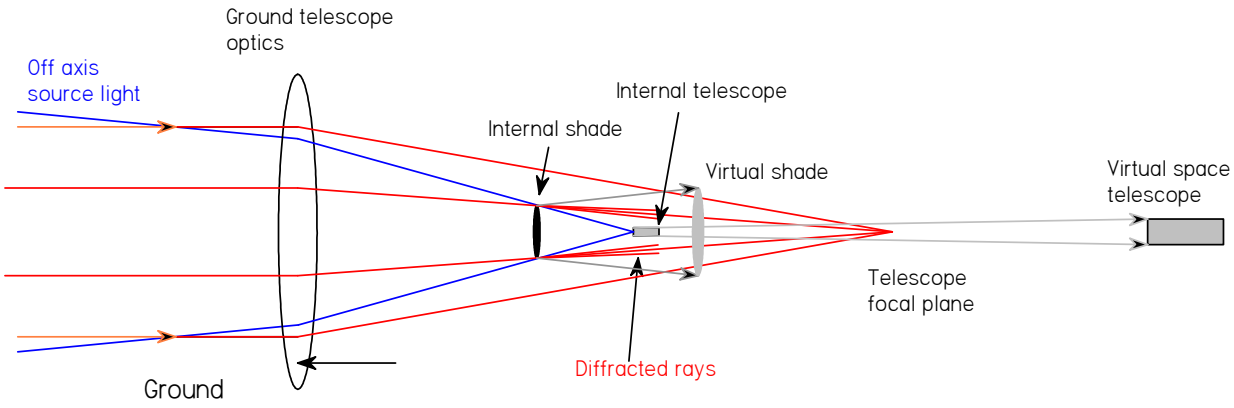

Figure 9: Internal starshade and virtual telescope.

Figure 10 shows the location of the virtual starshade at 1.2 micron wavelength on the same graphs as figure 1. The large starshade radius and large effective separation place this shade nearer to the flight model than any experiments to date for these two important parameters.

4. Possible Astronomical Targets

Possible targets include substellar companions (exoplanets), binary systems, and debris discs. To evaluate potential targets we assume deepest contrast of 10^{-8} (admittedly ambitious, but we find targets with much more favorable contrast), IWA 3 arc sec, OWA 15 arc sec and wavelength 1.5 to 1.8 um.

Substellar companions

Given the large IWA, targets would be self-luminous planets around young stars and very extended disks.

1- Known exoplanets and brown dwarfs in wide orbits around young stars

HD 106906b: A 11+/- 2 mJ companion orbits at 7.1" from this ~13 Myr old F5V star. Just 10^{-4} contrast given the high mass and young age. Should be straightforward, and other companions might be found down to 10^{-8} contrast. It also has a disk extending to 5" west in HST images.

GJ504b (~160Myr old): Jovian exoplanet with 3 x 10^{-7} H-band contrast at 2.5" (46 AU). So this is close-in but it may be possible to find fainter outer planets in this system. By pushing down the wavelength to 1.2 um to achieve a smaller IWA on the Hale telescope or by using the Gemini telescope, this should be possible.

HIP 78530b: ~23 mJ brown dwarf at 4.5" (710 AU). H band contrast is just 1000:1 around this very young star (~11Myr old).

2. Young compact binary systems

These observations would be aimed at verification of the improved resilience of the starshade's contrast to source extension. The presence of a companion at a small enough fraction of the IWA (say < 10%) should not create more leakage: it makes the shadow narrower but not brighter. It would be nice to demonstrate this property on the sky. If this was applied to young stars, there may be sufficient sensitivity to detect sub-stellar companions. A good place to do this would be in the nearby Scorpius-Centaurus OB Association. The revised ages for these 3 clusters are US (Upper Sco): 11 Myr, UCL (Upper Centaurus Lupus): 16 Myr, and LCC (Lower Centaurus Crux) 17 Myr. Most late A /early B stars in there are magnitude 5 to 7 at V and H, and sufficiently bright (see final table of Ref. 12). The best young close binary targets in there are: HIP 61639, 64515, 65089, 75210, 75476, 76071, 77939 (US), 78754, 79250 (US), 80126 (US), 80425 (US), 80461 (US). This list can be refined based on age (US young region is better) IR excess strength, since such exoplanets are apparently more often found around very massive disks.

In fact, both HD106906 and HIP78530 in category 1 above are also in this young stars OB association. So this appears to be a good place to look for substellar companions in wide orbits.

3. Extended disks

Starshade observations may bring higher rejection of the central star at 3"+. Usual disks with extension in the 3" to 15" range, and V mag < 8 for good AO correction are: Beta Pic (26" disk diameter), HD 15115 (19" disk diameter), HD 32297 (5.8", may be too small), HD 141569 (7.5") very interesting, see Ref. 14 on Gemini for current state of the art coronagraphic observations at H-band, AB Aur (18"), MWC 480 (8"), HD 92945 (10"), Eta Crv (11"), 61 Vir (22"), AU Mic (29"). Fomalhaut is mostly outside the OWA.

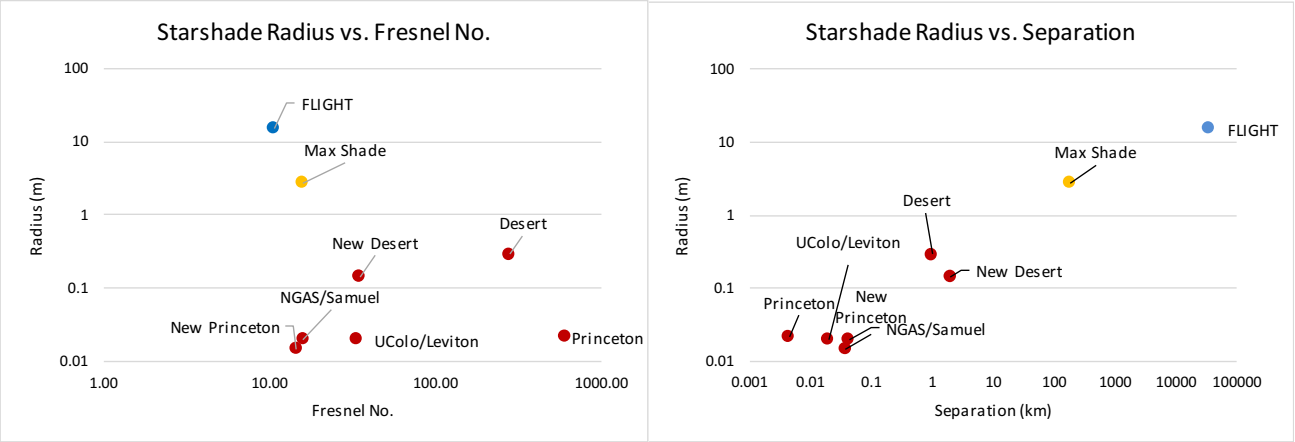

Figure 10: State of the art in ground tests (from Figure 1) with added prospective data for a shade equivalent to the Gemini shade at 1.2 micron from Table 2 (annotated Max Shade). Left: Max Shade radius is about one order of magnitude from flight. Right: Max Shade starshade-telescope separation improves on existing art by about two orders of magnitude.

CONCLUSION

For ground based starshades utilizing significant path lengths across the ground, a reasonable limit seems to be less than a 6000 m range under good atmospheric conditions, corresponding to a starshade diameter of ~0.31 m at $\aleph = 8$.

For the telescope scenarios, use of the ISI with its Pfund telescope (or in an equivalent setup, the McMath Solar Telescope) could reach 16,700 m range with a 0.57 m diameter shade, achieving a 3.5” IWA.

Use of a telescope AO system such as the Palomar PALAO could reach an IWA of between 2.2” and 3.3” with a 1.8 m starshade. The larger Gemini (or equivalent) telescope could reach an IWA between 1.5” and 2.2” with a 2.7 m starshade, significantly improving on existing experiments in both starshade size and range.

A realistic way forward for ground-based starshade experiments seems to be to minimize ground path length by using virtual telescope geometries in conjunction with existing ground-based large telescope facilities.

APPENDICES

A. KEY TO FIGURE 1 DATA

New Princeton, Ref. 16. NGAS/Samuel, Ref. 17. New Desert, Ref. 18. UColo/Leviton, from Table 1, row 1, raw data, Ref. 19. Desert, Ref. 20. Princeton, Ref. 21. Flight, Ref. 22.

ACKNOWLEDGEMENTS

This work was conducted at the Jet Propulsion Laboratory, California Institute of Technology, under contract with the National Aeronautics and Space Administration.

REFERENCES

1. D. Sirbu, N. Kasdin, and R. Vanderbei, Laboratory verification of high-contrast imaging with an occulter," Optics Express 21, 2013.

2. Tiffany Glassman, Suzanne Casement, Steve Warwick, Megan Novicki, “Measurements of high-contrast starshade performance”. Proc. SPIE 9143: Space Telescopes and Instrumentation 2014.

3. A.L. Buck, “Effects of the Atmosphere on Laser Beam Propagation”, Vol. 6, No. 4, Applied Optics, April 1967

4. Hervé Trinquet and Jean Vernin, “Using meteorological forecasts to predict astronomical ‘seeing’”, 11 June 2009, SPIE Newsroom.

5. Donald L. Walters and L. William Bradford, “Measurements of r0 and θ_0: two decades and 18 sites”, Applied Optics 36, No. 30, October 1997.

6. http://isi.ssl.berkeley.edu/

7. http://www.astro.caltech.edu/~lah/ay122/ay122.ao.part3.pdf

8. Absil, Olivier and Mawet, Dimitri, “Formation and evolution of planetary systems: the impact of high-angular resolution optical techniques” The Astronomy and Astrophysics Review18.3 (Jul 2010): 317-382.

9. Direct Imaging of a Cold Jovian Exoplanet in Orbit Around the Sun-Like Star GJ 504. M. Kuzuhara et al. Astrophysical Journal 774, 11, 2013.

10. HD 106906b: A Planetary-Mass Companion Outside A Massive Debris Disk, Vanessa Bailey et al. The

Astrophysical Journal Letters, Volume 780, Issue 1, article id. L4, 6 pp. (2014).

11. Discovery Of A ~23 mJup Brown Dwarf Orbiting ~700 Au From The Massive Star Hip 78530 In Upper Scorpius David Lafrenière et al. The Astrophysical Journal, 730:42, March 2011.

12. The primordial binary population 1. A near-infrared adaptive optics search for close visual companions to A star members of Scorpius OB2. M. B. N. Kouwenhoven et al. A&A 430, 137–154 (2005)

13. A brown dwarf desert for intermediate mass stars in Scorpius OB2? M. B. N. Kouwenhoven et al. A&A 464, 581–599 (2007)

14. The Gemini NICI Planet-Finding Campaign: asymmetries in the HD141569 disc. Beth A. Biller et al. Monthly Notices of the Royal Astronomical Society, Volume 450, Issue 4, p.4446-4457.

15. MNRAS 450, 4446–4457 (2015)

16. Private communication.

17. Rocco Samuele ; Tiffany Glassman ; Adam M. J. Johnson ; Rupal Varshneya ; Ann Shipley. Proc. SPIE 7440, Techniques and Instrumentation for Detection of Exoplanets IV, 744004 (August 19, 2009)

18. Private communication.

19. "White light demonstration of one hundred parts per billion irradiance suppression in air by new starshade occulters" Douglas B. Leviton, Webster C. Cash, Brian Gleason, Michael J. Kaiser, Sarah A. Levine, Amy S. Lo, Eric Schindhelm, Ann F. Shipley, UV/Optical/IR Space Telescopes: Innovative Technologies and Concepts III edited by Howard A. MacEwen, James B. Breckinridge. Proc. of SPIE Vol. 6687, 66871B, (2007)

20. Private communication.

21. "Optical verification of occulter-based high contrast imaging" Dan Sirbu ; Eric J. Cady ; N. Jeremy Kasdin ; Robert J. Vanderbei ; Jianxiao Lu ; Emmeline Kao. Proc. SPIE 8151, Techniques and Instrumentation for Detection of Exoplanets V, 815114 (September 15, 2011)

22. "Exo-S: Starshade Probe-Class Exoplanet Direct Imaging Mission Concept", Final Report, ExoPlanet Exploration Program, Astronomy, Physics and Space Technology Directorate, Jet Propulsion Laboratory for Astrophysics Division Science Mission Directorate NASA, March 2015.

BIOGRAPHY